Renewable Energy 147 (2020) 916–923

Contents lists available at ScienceDirect

Renewable Energy

journal homepage: www.elsevier.com/locate/renene

Cascade conversion of furfural to fuel bioadditive ethyl levulinate over bifunctional zirconium-based catalysts

Mengzhu Li [a], Junnan Wei [a], Guihua Yan [a], Huai Liu [a], Xing Tang [a, b, *], Yong Sun [a, b], Xianhai Zeng [a, b], Tingzhou Lei [c], Lu Lin [a, b, **]

[a] Xiamen Key Laboratory of Clean and High-valued Applications of Biomass, College of Energy, Xiamen University, Xiamen, 361102, China
[b] Fujian Engineering and Research Center of Clean and High-valued Technologies for Biomass, Xiamen, 361005, Fujian, China
[c] Henan Key Lab of Biomass Energy, Henan, 450008, China

ARTICLE INFO

Article history:
Received 12 March 2019
Received in revised form
12 July 2019
Accepted 14 September 2019
Available online 16 September 2019

Keywords:
Furfural
Ethyl levulinate
Transfer hydrogenation
Ethanolysis
Bimetallic catalyst
Fuel bioadditive

ABSTRACT

Biomass-derived ethyl levulinate (EL) is currently deemed as a promising fuel bioadditive to improve (bio)diesel combustion performance without the sacrifice of its octane number. In this contribution, a range of Zr–Al bimetallic catalysts were prepared for the cascade conversion of furfural to EL by the integration of transfer hydrogenation and ethanolysis in ethanol. The ratio of Lewis to Brønsted acid sites (L/B) could be tuned by the ratio of Al_2O_3 to ZrO_2 over SBA-15 support. Among these catalysts, Zr–Al/SBA-15(30:10) with appropriate L/B ratio of 2.25 exhibited an outstanding catalytic performance to give a furfural (FF) conversion up to 92.8% with a EL selectivity as high as 71.4% at 453 K in 3 h.

1. Introduction

Biomass is the only renewable carbon resource that can be converted into liquid fuels to replace petroleum-based counterparts [1–5]. At this point, biomass-derived ethyl levulinate (EL) has been currently put forward as a promising bio-based diesel additive [6,7]. The addition of EL is able to greatly improve the cold flow properties of biodiesel, and the blended biodiesel fuel with EL meets the biodiesel standard of ASTM D6751 [8,9]. EL can also be served as a fuel oxygenate for regular diesel, as it can bring about significant decrease in the emission of hydrocarbon and CO [10,11]. In addition, EL can be employed as the starting material for producing numerous value-added chemicals, for instance, γ-valerolactone (GVL) [12], 1,4-pentanediol (1,4-DPO) [13] and pyrrolidone [14].

It is known that EL can be easily produced by acid-catalyzed alcoholysis of bio-derived carbohydrates (e.g. cellulose, glucose or fructose) in ethanol [15–18]. Nevertheless, the above strategy suffers from poor solubility of carbohydrates in ethanol, relatively poor EL yield with the formation of intractable humins [19,20]. To this end, the conversion of FF or furfuryl alcohol (FA) to EL is recently gaining momentum, because FF or FA is available on an industrial scale from feedstock like corncob and has good solubility in most solvents [21]. Therefore, FF or FA is a promising alternative for the production of EL in a commercial scale. The transformation of FA, the product of the hydrogenation of FF, to EL with a desirable yield is well established by acid-catalyzed ethanolysis [22]. The one-pot conversion of FF to EL is highly desirable but challenging, which requires the integration of the hydrogenation of FF to FA and the subsequent ethanolysis of FA. The top challenge for the transformation of FF to EL is the preparation of efficient bifunctional catalysts that are able to offer desirable selectivity towards EL [23]. However, this above promising topic is still mostly uncharted territory.

Recently, Chen *et.* prepared a bifunctional catalyst $Pt/ZrNbPO_4$ for the hydrogenation of FF to FA and the subsequent ethanolysis of FA to EL under external hydrogen atmosphere, which gave the optimized FF conversion of 92.3% with a EL selectivity of 75.7%

* Corresponding author. Xiamen Key Laboratory of Clean and High-valued Applications of Biomass, College of Energy, Xiamen University, Xiamen, 361102, China.
** Corresponding author. Xiamen Key Laboratory of Clean and High-valued Applications of Biomass, College of Energy, Xiamen University, Xiamen, 361102, China.
E-mail addresses: x.tang@xmu.edu.cn (X. Tang), lulin@xmu.edu.cn (L. Lin).

https://doi.org/10.1016/j.renene.2019.09.064
0960-1481/

(403 K, 5 MPa H_2, 6 h) [24]. Given ethanol employed as the reaction medium, catalytic transfer hydrogenation through Meerwein–Ponndorf–Verley (MPV) reduction for the conversion of FF to FA is deemed as an appealing alternative by using ethanol as in-situ hydrogen-source [25]. In addition, the use and management of liquid alcohols is more convenient as compared to molecular H_2 [26,27]. In this light, Au–$H_4SiW_{12}O_{40}/ZrO_2$ was prepared for the formation of EL from FF in ethanol through MPV reduction and ethanolysis in series, which could offer a desirable EL yield of 77.6% (393 K, 24 h) [28]. In this case, Au and $H_4SiW_{12}O_{40}$ catalyzed the MPV reduction of FF and the ethanolysis of FA, respectively. To the best of our knowledge, non-noble catalysts are more desirable from the perspective of economy. Depending on this, Peng and co-workers developed a mixed catalysts system comprising of Zr-MCM-41 and Amberlyst-15, which could give a yield of isopropyl levulinate as high as 85.3% in isopropanol with no external hydrogen (403 K, 24 h) [29]. However, this mixed catalysts system failed to offer a great EL yield in ethanol under the same conditions. More recently, T. Kan et al. revealed that the conversion of FF to EL by using the mixture of Zr/SBA-15 and ZSM-5 as catalyst, and gave an EL yield of 55% at 453 K in 8 h [30]. This above EL yield is still largely lower than that obtained over Au–$H_4SiW_{12}O_{40}/ZrO_2$ (77.6%) [28]. On the other hand, a noble-metal-free bi-functional catalyst is a more appealing option as compared to the mixed catalytic system.

SBA-15, one of Santa Barbara amorphous materials, is the ordered mesoporous silicas with high surface areas, large pore sizes and volumes, which offers an opportunity to enhance the accessible active sites and thermal stability. Therefore, SBA-15 is recognized as the promising and robust catalyst support [31]. It's generally accepted that Lewis acid drives the MPV reduction of FF to FA, and Brønsted acid facilitates the ethanolysis of FA to EL [32]. In this study, we prepared a bimetallic oxide supported on SBA-15 catalysts (Zr–Al/SBA-15), in which ZrO_2 with Lewis acid sites meets the requirement for the MPV reduction of FF to FA, Al_2O_3 with Brønsted acid sites is charge of alcoholysis of FA to EL in ethanol. The ratio of Lewis and Brønsted acid sites could be flexibly tuned via adjusting the ratio of ZrO_2 to Al_2O_3, resulting in a desirable EL yield up to 67.2% from FF. To the best of knowledge, this (67.2%) is the highest EL yield derived from FF over non-noble metal catalysts (Table S1). Accordingly, a facile one-pot conversion of FF to EL can be developed through the integration of MPV reduction and alcoholysis over bifunctional Zr–Al/SBA-15 catalyst.

2. Experiment

2.1. Chemicals and materials

FF (98%), FA (98%), EL (98%), GVL (98%), 2-(diethoxymethyl)furan (DTMF, 98%), $Zr(NO_3)_4{\cdot}5H_2O$ (99%), and $Al(NO_3)_3{\cdot}9H_2O$ (99%) were bought from Aladdin Reagent Co. Ltd. (Shanghai, China). Ethyl furfuryl ether (EFE, 98%) was purchased from Energy Chemical Co. Ltd. (Shanghai, China). SBA-15, MCM-41, USY, and MCM-41 were obtained from Nanjing JCNANO Technology Co. Ltd (Nanjing, China). ZrO_2 and Al_2O_3 was obtained by the calcination of $Zr(NO_3)_4{\cdot}5H_2O$ and $Al(NO_3)_3{\cdot}9H_2O$ at 823 K. Notably, FF was purified by distillation before use.

2.2. Catalysts preparation

An incipient wetness impregnation method was introduced to load 40 wt % active metal oxides over SBA-15 [33–35]. The resulting catalyst is hereafter denoted as metal/SBA-15 (x: y), in which x or y represents the mass ratio of metal oxide to SBA-15. The typical procedure for the synthesis of Zr–Al/SBA-15(30:10) is described below: 0.523 g $Zr(NO_3)_4{\cdot}5H_2O$ and 0.184 g $Al(NO_3)_3{\cdot}9H_2O$ were first dissolved into 2.7 mL deionized water, and the obtained salt solution was transferred dropwise onto 0.5 g SBA-15, followed by the impregnation for 8 h at room temperature. The catalyst precursor was obtained after drying at 383 K overnight in an oven, and further calcined at 823 K for 5 h.

2.3. Catalyst characterization

X-ray diffraction (XRD) patterns were carried out by a Panalytical X'pert Pro diffractometer (40 kV, 30 mA, 10° min^{-1}, $2\theta = 20°–70°$). Small-angle X-ray scattering (SAXS) was conducted on Rigaku Ultima IV diffractometer (35 KV, 15 mA, DHL = 5 mm, 1° min^{-1}, $2\theta = 0.5°–6°$). The specific surface area, pore volumes, and average pore size of catalyst were counted by BET (Brunauer–Emmett–Teller) and BJH (Barret–Joyner–Halenda) method with Micromeritics ASAP 2020 HD88. The temperature-programmed desorption of ammonia (NH_3-TPD) was carried on AutoChem 2920 (Micromeritics), gave the surface acidity of the catalysts. Scanning electron microscope (SEM) images were collected on a SUPRA 55 at 5 KV. Pyridine-adsorbed Fourier transform infrared spectroscopy (Py-FTIR) was used to gain acid properties of the catalysts. The results were recorded by Bruker Tensor 27 spectrometer. Before the analysis, 30 mg sample was pressed into the disc with the diameter of 13 mm and then treated at 623 K for 4 h in a vacuum. Pyridine was introduced to contact with the sample for 20 min when the sample was cooled down to room temperature and then evacuated pyridine for 30 min. Following which, the sample was heated at 623 K at a heating rate of 10 K/min for 30 min, and the spectra was recorded. Samples for SEM images were deposited on Si wafers. High Resolution Transmission Electron Microscope (HRTEM) images were performed by JEM-2100 (200 KV). X-ray photoelectron spectroscopy (XPS) data was carried out on a PHI 5000 VB III.

2.4. Catalytic conversion of FF into EL

The cascade conversion of FF to EL was conducted in a 50 mL stainless steel reactor. Typically, 0.2 g furfural, 20 mL ethanol and 0.1 g catalyst powder were transferred into the reactor, followed by sealing and purging with N_2 for four times. Then, the reactor was heated to the required reaction temperature for a given time in the heating jacket. After the reaction stopped, the reactor was immediately taken out from the heating jacket and cooled down to room temperature. Then, the reactor was opened, and the resulting liquid product and solid catalyst were separated by filtration. The liquid product was analyzed by gas chromatography (GC) and gas chromatography-mass spectrometry (GC-MS), and the spent catalyst was washed with ethanol and dried at 333 K for 6 h.

2.5. Sample analysis

The liquid was qualitatively analyzed by GC-MS (Thermo Trace 1300 and ISQ LT). The quantitative analysis of the liquid product was conducted on a GC Agilent 7890. The temperature program was as follows: 313 K (4 min) − 15 K/min − 523 K (5 min). FF conversion (X_{FF}, %), the selectivity and yield of different products (S_P, % and Y_P, %) were calculated using the followed equations (1)–(3):

$$X_{FF}\,(\%) = (1 - \text{moles of FF in product} / \text{initial moles of FF}) \times 100\% \quad (1)$$

$$Y_P\,(\%) = (\text{moles of P in product} / \text{initial moles of FF}) / X_{FF} \times 100\% \quad (2)$$

$$S_P\,(\%) = Y_P / X_{FF} \times 100\%\ (\text{P} = \text{FA, EL, GVL, etc.}) \quad (3)$$

3. Results and discussion

3.1. Catalyst characterization

3.1.1. Crystallinity

For neat SBA-15, the wide-angle XRD pattern exhibited the characteristic peak of amorphous silica at $2\theta \approx 23.5^\circ$ (Fig. 1A(a)) [36], whereas no characteristic peak of alumina for Al/SBA-15(40) was observed (Fig. 1A(b)), indicating the highly dispersion of alumina on SBA-15. In contrast, Zr/SBA-15(40) showed six obvious peaks for ZrO_2 (Fig. 1A(f)). For instance, the peaks at 28.2° and 31.5° suggested the presence of monoclinic zirconia (JCPDS no. 13–307), and the peaks at 30.3°, 34.3°, 50.3° and 60.1° were allocated to the tetragonal zirconia (JCPDS no. 17–923) [37,38]. With the increasing amount of Al_2O_3, the diffraction peaks for ZrO_2 became weak and even disappeared finally for Zr–Al/SBA-15 catalyst (Fig. 1A(c-e)), which implied that the dispersion of ZrO_2 was probably improved with the incorporation of Al_2O_3. Additionally, these findings also suggested the small particle size of ZrO_2 in Zr–Al/SBA-15 catalysts than that in Zr/SBA-15(40).

Fig. 1B showed the SAXS patterns of catalysts. SBA-15 showed three well-resolved peaks centered at $2\theta = 0.92^\circ$, 1.57°, and 1.82° which represent (100), (110), (200) reflections of the 2-D hexagonal lattice symmetry, respectively [39]. Apparently, the intensity of the characteristic reflections for SBA-15 considerably decreased in Zr–Al/SBA-15(20:20), Zr–Al/SBA-15(25:15) and Zr/SBA-15(40), elucidating that the mesoporous channels of SBA-15 was filled with these metal oxides [40]. On the contrary, distinct (100), (110), (200) reflections for SBA-15 were observed in Zr–Al/SBA-15(30:10), suggesting that the mesoporous channels of SBA-15 kept almost intact in this case. Notably, the above three peaks shifted to higher angles for Zr–Al/SBA-15 catalysts, which implied that the partial metal oxides were probably embedded into the inner walls of the SBA-15 channels [41].

3.1.2. Surface area and porosity

As shown in Fig. S1, all the catalyst solids displayed typical type-IV profiles for the N_2 adsorption-desorption isotherms, indicating that SBA-15 mesoporous structure retained after loading metal oxides. BET surface areas, pore volumes, and the average pore size of catalysts were listed in Table 1. Pure SBA-15 exhibited the highest specific surface area (S_{BET}: 509.85 m^2/g), pore volume (V_{pore}: 0.97 m^3/g) and average pore diameter (D_{pore}: 7.60 nm). The loading of Al_2O_3 or ZrO_2 resulted in pronounced decrease in the specific surface area of monometallic oxide supported on SBA-15. To be specific, the specific surface areas of Al/SBA-15(40) and Zr/SBA-15(40) were measured as 396.93 m^2/g and 464.83 m^2/g, respectively (Table 1, entries 2 & 6). The decrease could be attributed to the deposition of partial metal oxide particles onto the internal surface or the pore entrance of the SBA-15 channels [42]. Interestingly, supported bimetallic oxide catalysts gave a specific surface area between those of the above two monometallic oxide catalysts (Table 1, entries 3–5). For example, Zr–Al/SBA-15(30:10) displayed a specific surface area of 442.09 m^2/g (Table 1, entry 5). In addition, analogous phenomena were also observed in the pore volume and the average pore size of these catalysts (Table 1).

Table 1
Textural properties of different catalysts.

Entry	Catalyst	S_{BET}, m^2/g	V_{pore}, cm^3/g	D_{pore}, nm
1	SBA-15	509.85	0.97	7.60
2	Al/SBA-15(40)	396.93	0.48	4.85
3	Zr–Al/SBA-15(20: 20)	443.63	0.63	5.71
4	Zr–Al/SBA-15(25: 15)	409.21	0.52	5.05
5	Zr–Al/SBA-15(30: 10)	442.09	0.61	5.51
6	Zr/SBA-15(40)	464.83	0.70	6.01

3.1.3. Surface acidic property

The surface acidic property of the catalysts was analyzed by

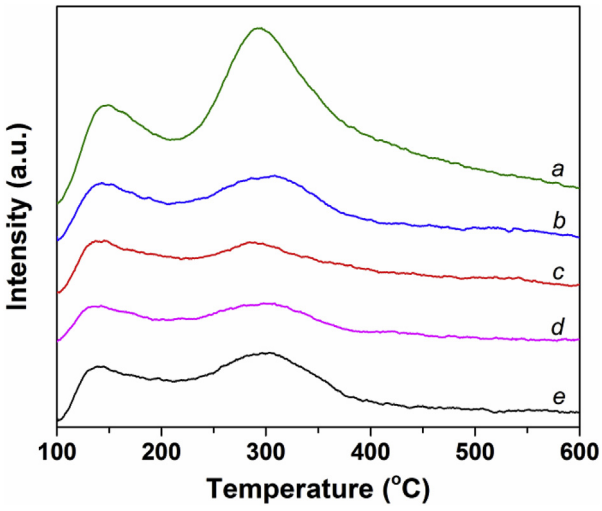

Fig. 2. NH_3-TPD profiles of (a) Al/SBA-15(40), (b) Zr–Al/SBA-15(20:20), (c) Zr–Al/SBA-15(25:15), (d) Zr–Al/SBA-15(30:10), (e) Zr/SBA-15(40).

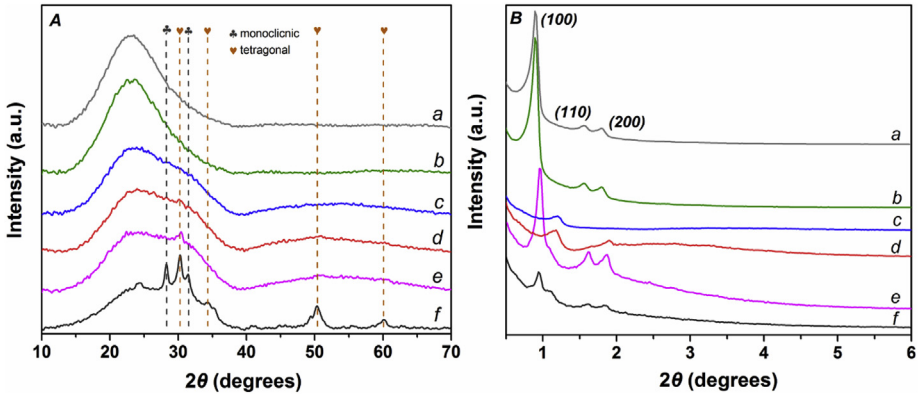

Fig. 1. A: Wide-angle XRD (A) and SAXS (B) patterns for (a) SBA-15, (b) Al/SBA-15(40), (c) Zr–Al/SBA-15(20:20), (d) Zr–Al/SBA-15(25:15), (e) Zr–Al/SBA-15(30:10), (f) Zr/SBA-15(40).

NH_3-TPD. As shown in Fig. 2, all the samples had two desorption peaks centered at 130 °C and 300 °C, corresponding to the weak acid sites and the medium acid sites, respectively. Al/SBA-15(40) exhibited the most intense NH_3 desorption peaks among these samples, suggesting the largest amount of acid sites in Al/SBA-15(40) (Fig. 2a). Furthermore, compared with Al/SBA-15(40) and Zr/SBA-15(40), Zr–Al/SBA-15 catalysts showed weaker desorption peaks (Fig. 2c–d), implying that the amount of acid sites decreased in the bimetallic oxide catalysts.

The type of acid site of these catalysts were characterized by Py-FTIR. As manifested in Fig. S2, both Lewis and Brønsted acid sites were observed in all the samples of Py-FTIR spectra. Lewis acid and Bronsted acid were quantitated by fitting deconvolution of peaks at 1450 cm^{-1} and 1540 cm^{-1}, respectively. As shown in Table 2, Lewis acid sites are dominated in all the catalysts, especially for Zr/SBA-15(40), which provided the highest L/B ratio of 6.50 (Table 2, entry 4). Monometallic oxide catalysts, especially for Al/SBA-15(40), possessed more Lewis sites compared to bimetallic oxide catalysts. Al/SBA-15(40) also showed the highest amount of Brønsted sites (Table 2, entry 1), which gradually decreased with the increasing ZrO_2 content (Table 2, entries 2–4), indicating that there was interaction between Al and Zr species. Notably, Zr–Al/SBA-15(30:10) had the lowest total acid sites among all the catalysts (Fig. 2d), but offered a moderate L/B ratio of 2.25 (Table 2, entry 3).

3.1.4. Surface morphology

The HRTEM images of SBA-15 and Zr–Al/SBA-15(30:10) in the pore axis and the pore vertical were also provided in Fig. 3. Both SBA-15 and Zr–Al/SBA-15(30:10) exhibited similar ordered array of uniform mesoporous channels with p6mm hexagonal symmetry [43], indicating that the fundamental frame of SBA-15 retained after loading metal oxides. This result was well in line with the characterization of SAXS and N_2 adsorption-desorption isotherms (Fig. 1B and Fig. S1). Additionally, no visible metal oxide particles were observed in HRTEM images and SEM images of Zr–Al/SBA-15(30:10) (Fig. 3 and Fig. S3), implying that the homogenous dispersion of metal oxides. The elemental mapping analysis also reinforced the above observation (Fig. S4).

3.1.5. XPS analysis

XPS was used to investigate the surface elemental chemical status. As illustrated in Fig. S5, Zr, Al, Si and O were observed in the XPS spectrum of Zr–Al/SBA-15 samples. As shown in Fig. 4A, all the Zr 3d spectra of these samples exhibited double centers assigning to $3d_{3/2}$ and $3d_{5/2}$, resulting from spin–orbit components of zirconium [44]. Compared to Zr/SBA-15(40), the binding energy of Zr 3d slightly shifted to higher values for all Zr–Al/SBA-15 samples (Fig. 4A). On the contrary, the binding energy of Al 2p or O 1s for Zr–Al/SBA-15 samples slightly shifted to lower values as compared to that of Al/SBA-15(40) (Fig. 4B). Apparently, there is interaction between Al and Zr species, which should responsible for the shift of binding energy for Zr 3d, Al 2p and O 1s. The formation of Zr–O–Al probably occurred in Zr–Al/SBA-15 samples [45], which further

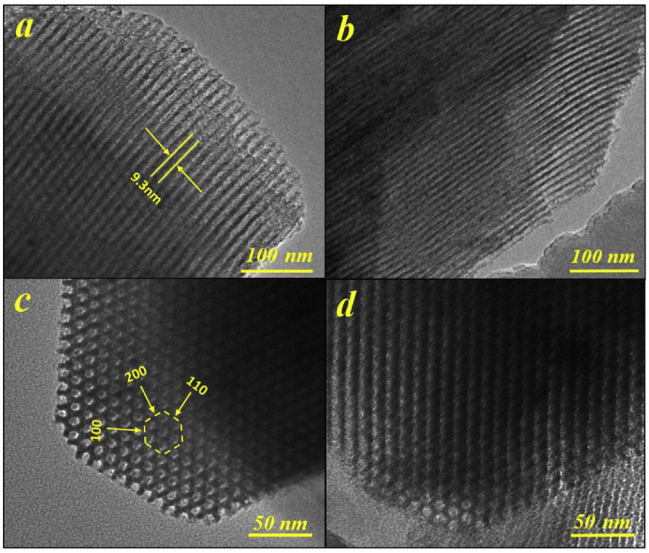

Fig. 3. HRTEM images of SBA-15 (a and c) and Zr–Al/SBA-15(30:10) (b and d).

brought about the decrease of acidic sites in Zr–Al/SBA-15 catalysts (Table 2 and Fig. 2). In addition, the surface elemental composition of Zr–Al/SBA-15(30:10) was also measured by XPS analysis, and the surface Zr/Si molar ratio of 0.046 was obtained, which is lower than the integral molar ratio of 0.146. This finding indicated that metal oxide particles were mainly supported on the inside of the SBA-15 channel, which is in accordance with SAXS result (Fig. 1).

3.2. Catalyst screening

The reaction pathway for the cascade conversion of FF to EL by using ethanol as hydrogen donor was depicted in Scheme 1. The cascade process started with the transfer hydrogenation of FF to FA promoted by Lewis acid. In parallel, partial FF could convert into DTMF by the reversible acetalization with ethanol [30]. Subsequently, EFE was produced through the etherification of FA with ethanol over Lewis or Brønsted acid. For the next step, EFE could convert to the desirable product EL by hydrolytic ring-opening reaction in the presence of Brønsted acid. Besides, EL could go through the deep transfer hydrogenation to form GVL over Lewis acid. The formation of humins by the condensation of FF or FA could also take place in the presence of acid catalysts.

The preliminary catalyst screening experiments were conducted at 423 K in 5 h (Table S2 & Table 3). As summarized in Table S2, the choice of support and the-second metal was efficient on the catalytic performance for the reaction of FF to EL. The exclusive product DTMF could be detected in the presence of pure SBA-15 or without any catalyst (Table 3, entries 1–2), suggesting that SBA-15 was not able to catalyze the transfer hydrogenation of FF. Both ZrO_2 and Al_2O_3 could offer near-100% conversion of FF with FA as the main

Table 2
Distribution of Lewis and Brønsted acid sites of different catalysts[a].

Entry	Catalyst	Lewis sites, μmol/g	Brønsted sites, μmol/g	L/B ratio
1	Al/SBA-15(40)	0.22	0.12	1.83
2	Zr–Al/SBA-15(20:20)	0.12	0.07	1.71
3	Zr–Al/SBA-15(30:10)	0.09	0.04	2.25
4	Zr/SBA-15(40)	0.13	0.02	6.50

[a] Lewis acid and Bronsted acid were quantitated by fitting deconvolution of peaks at 1450 cm^{-1} and 1540 cm^{-1} respectively in Fig. S2.

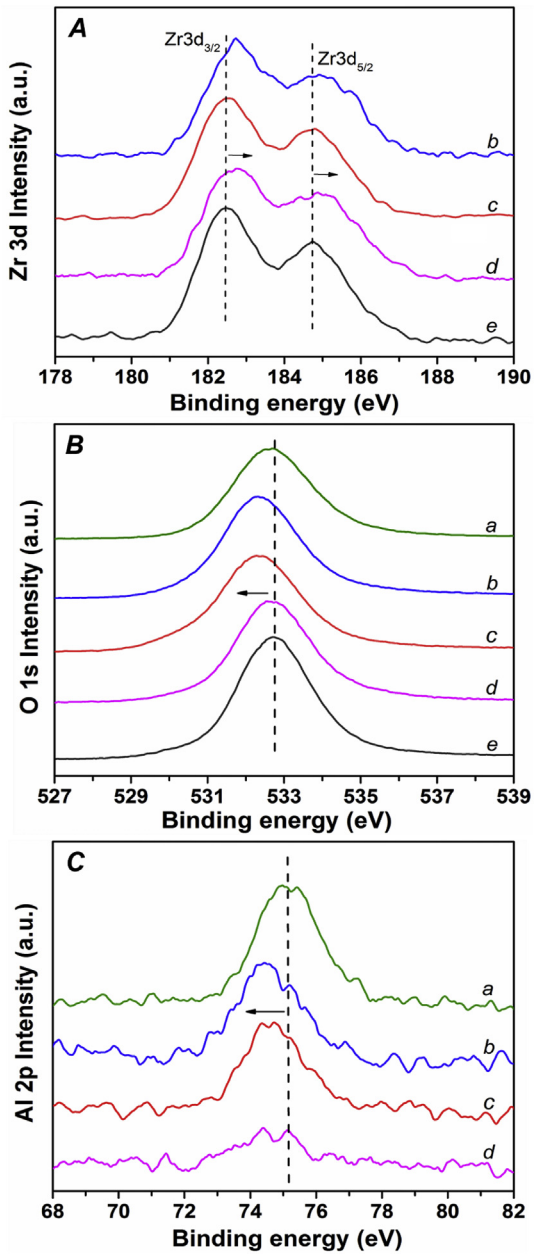

Fig. 4. XPS spectra of high-resolution (A) Zr 3d, (B) O 1s and (C) Al 2p: (a) Al/SBA-15(40), (b) Zr–Al/SBA-15(20:20), (c) Zr–Al/SBA-15(25:15), (d) Zr–Al/SBA-15(30:10), (e) Zr/SBA-15(40).

product, but no EL or EFE was detected in these cases (Table 3, entries 3–4). This observation indicated that ZrO_2 and Al_2O_3 only possessed Lewis acid sites, which was able to catalyze the catalytic transfer hydrogenation of FF. Interestingly, EL was formed with no FA detected in the product under the same reaction conditions, once ZrO_2 and/or Al_2O_3 were/was supported on SBA-15 (Table 3, entries 5–9), which should be attributed to the generation of Brønsted acid sites on the supported metal oxide catalysts on SBA-15 (Table 2). If FA was applied as the starting material in the presence of Zr–Al/SBA-15(30:10), a complete FA conversion with EL yield of 84.1% was obtained (Table 3, entry 10), indicating that the conversion of FA is a fast step.

Additionally, Al/SBA-15(40) and Zr/SBA-15(40) offered near-100% FF conversion, whereas Zr–Al/SBA-15 catalysts only provided FF conversion lower than 75% (Table 3, entries 5–9). Apparently, Al/SBA-15(40) and Zr/SBA-15(40) had an abundance of acidic sites especially Lewis acid (Table 2), which should responsible for the high FF conversion. It was noticed in Table 3 that the total selectivity of products in the presence of Al/SBA-15(40) was only 76.7% (Table 3, entry 5), probably because excessive Lewis and Brønsted acid sites in Al/SBA-15(40) promoted the side reactions of FA to form humins. However, Zr–Al/SBA-15(20:20) also possessed a wealth of acidic sites, but gave the lowest FF conversion of 58.9% among all the metal oxide supported catalysts (Table 3, entry 6). On the other hand, EL selectivity failed to be proportional to the amount of acidic sites of the catalysts. For instance, Zr–Al/SBA-15(30:10) with the least acidic sites (Table 2, entry 3) afforded the highest EL selectivity (Table 3, entry 8). What also should be paid attention to was that Zr/SBA-15(40) offered a considerable total selectivity of products with a lower selectivity of EL compared to that of Zr–Al/SBA-15(30:10) (Table 3, entries 8 & 9), probably because Zr/SBA-15(40) had no enough Brønsted acid sites to catalyze the ethanolysis of EFE (Table 2).

As shown in Scheme 1, the conversion of FF to EL contained several reaction steps, including catalytic transfer hydrogenation, etherification and ethanolysis. It was well known that catalytic transfer hydrogenation was driven by Lewis acid, and the subsequent etherification and ethanolysis were mainly catalyzed by Brønsted acid. According to Le Chatelier's principle, transfer hydrogenation of FF to FA could facilitate the following conversion of FA to EL by etherification and ethanolysis, the conversion of FA to EL in turn could promote the former reaction. Therefore, FF conversion and EL selectivity were not simply associated with the amount of acidic sites in the catalysts. We found that too high or too lower ratio of Lewis to Brønsted acid site (L/B ratio) resulted in a relatively poor EL selectivity in the cases of Al/SBA-15(40) and Zr/SBA-15(40) (Table 2, entries 1 and 4; Table 3, entries 5 and 9). Too high Brønsted acid amount lead the side reactions of FA and humins would be formed, but too low Brønsted acid amount couldn't catalyze the ethanolysis of EFE to obtain EL. Interestingly, Zr–Al/SBA-15(30:10) with appropriate L/B ratio gave the highest EL selectivity (Table 3, entry 8).

Reaction conditions: 0.2 g FF, 20 mL ethanol, 0.1 g catalyst, 423 K, 5 h and N_2 at atmospheric conditions. a: FA as substrate, b: FA conversion.

3.3. Effect of other reaction parameters

As illustrated in Fig. 5a, FF conversion improved from 68.5% to 98.2% along with the temperature increasing from 413 K to 463 K in the presence of Zr–Al/SBA-15(30:10). As the matter of fact, the maximum EL selectivity of 60.5% was achieved at 453 K with FF conversion up to 92%. Nevertheless, EL selectivity slightly declined to 54.2% with the formation of GVL at 463 K, indicating that elevated temperature facilitated the further transfer hydrogenation of EL to GVL. In addition, EL selectivity gradually increased at the cost of DTMF selectivity in the range of 413 K–453 K (Fig. 5a), clearly suggesting that the conversion of FF to DTMF was a reversible reaction (Scheme 1). The influence of reaction time was also evaluated at 453 K and the results were presented in Fig. 5b. Both FF conversion and EL selectivity improved with prolonging the reaction time from 1 to 3 h. Interestingly, FF conversion reached a plateau at 92.8% at 453 K in 3 h, whereas EL selectivity gradually decreased from 71.4% in 3 h–60.5% in 5 h. A small amount of GVL was also detected in a reaction time longer than 3 h, indicating that the transfer hydrogenation of EL to GVL occurred with prolonging

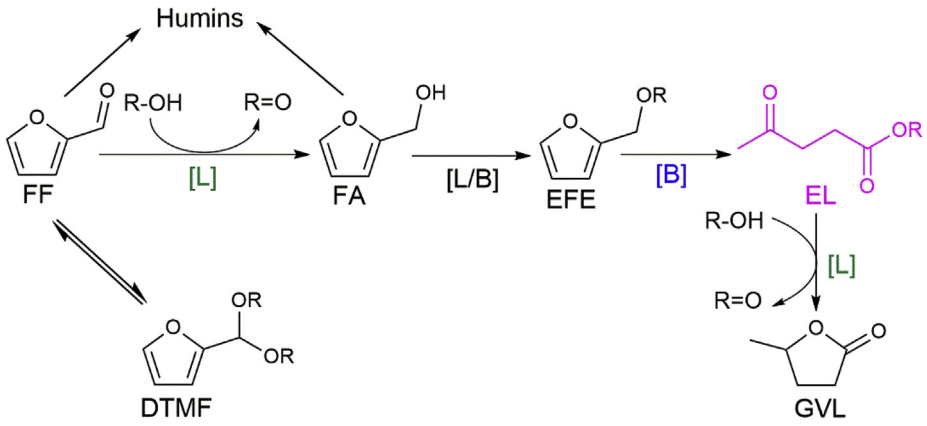

Scheme 1. Proposed reaction pathway of conversion FF into EL in ethanol. R = ethyl; [L] = Lewis acidity; [B] = Brønsted acidity.

Table 3
The cascade conversion of FF to EL over various catalysts.

Entry	Catalyst	X_{FF},%	S_{EL},%	S_{FA},%	S_{EFE},%	S_{DTMF},%	S_{Total},%
1	Blank	99.9	0	0	0	89.2	89.2
2	SBA-15	47.6	0	0	0	79.4	79.4
3	ZrO_2	95.8	0	82.9	0	1.1	84.0
4	Al_2O_3	99.9	0	93.6	0	5.2	98.8
5	Al/SBA-15(40)	99.9	22.7	0	10.1	43.9	76.7
6	Zr–Al/SBA-15(20:20)	58.9	24.1	0	5.8	23.6	53.5
7	Zr–Al/SBA-15(25:15)	63.0	24.6	0	15.4	36.0	76.0
8	Zr–Al/SBA-15(30:10)	73.5	42.6	0	9.4	40.5	92.5
9	Zr/SBA-15(40)	99.9	18.7	0	13.8	59.0	91.5
10[a]	Zr–Al/SBA-15(30:10)	99.9[b]	84.1	0	0	0	84.1

reaction time to 4 or 5 h. Manifestly, the total selectivity of detectable products was reduced with prolonging reaction time to 4 or 5 h, suggesting that more undetectable by-products humins formed in prolonged time.

The effect of the catalyst loading on the products selectivity and distribution was investigated at 453 K in 3 h. As shown in Fig. 6, FF conversion steadily increased with the increasing catalyst loading. In contrast, EL selectivity first reached the highest value of 71.4% at a catalyst loading of 50%, but then decreased with further increasing the catalyst loading. Interestingly, GVL selectivity sharply increased if a catalyst loading of greater than 50% was employed, implying that higher catalyst loading could provide more Lewis acid sites to promote the further transfer hydrogenation of EL to GVL.

3.4. Conversion of FF in different alcohols

Encouraged by the superior catalytic performance of Zr–Al/SBA-15(30:10) for the conversion of FF to EL in ethanol, other alcohols were also investigated as the solvent and H-donor. As shown in Table 4, all the alcohols offered a FF conversion greater than 90% at the same reaction conditions. However, alkyl levulinate (AL) was detected as the main product in primary alcohols, whereas GVL became the dominate product in secondary alcohols. For example, a AL selectivity of 52.2% with a GVL selectivity of 19.3% was achieved at 453 K in 3 h over Zr–Al/SBA-15(30:10) in 1-butanol (Table 4, entry 3). In comparison, a GVL selectivity of 39.2% with a AL selectivity of 19.5% was obtained in 2-propanol under the same reaction conditions (Table 4, entry 2). The product distribution of the conversion of FF in various alcohols was strongly associated with the reduction potential (△Ho f) of the alcohol applied. Generally, the lower △Ho f of the alcohol, the stronger ability to provide hydride ions for the transfer hydrogenation by using alcohol as the H-donor [46]. Therefore, the further catalytic transfer hydrogenation of EL to GVL was largely improved in secondary alcohols, such as 2-propanol or 2-butanol (Table 4, entries 2 and 4). In

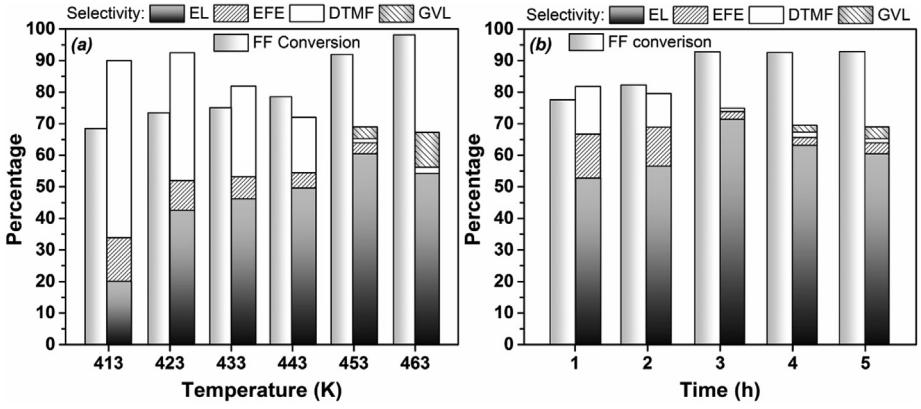

Fig. 5. Effect of reaction temperature (a) and reaction time (b) on FF conversion and product selectivity. Reaction conditions: 0.2 g FF, 20 mL ethanol, 0.1 g Zr–Al/SBA-15(30:10), N_2 at atmospheric conditions. (a) 5 h; (b) 453 K.

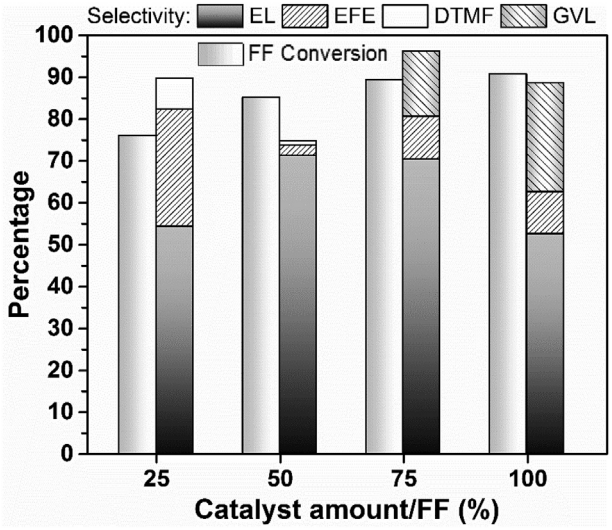

Fig. 6. Effect of catalyst dosage on the conversion of FF to EL. Reaction conditions: 0.2 g FF, 20 mL ethanol, Zr–Al/SBA-15(30:10), 453 K, 3 h and N_2 at atmospheric conditions.

Table 4
Synthesis of alkyl levulinates and GVL in various alcohols over Zr–Al/SBA-15(30:10).

Entry	Solvent	△Ho f[a]	X,%	Selectivity of products, %		
				AL	GVL	AL + GVL
1	Ethanol	85.4	92.8	71.4	0.0	71.4
2	2-Propanol	70.0	98.8	19.5	39.2	58.7
3	1-Butanol	79.7	97.5	52.2	19.3	71.5
4	2-Butanol	69.3	93.9	23.3	38.6	61.9

summary, these above findings indicated that Zr–Al/SBA-15(30:10) was a promising bifunctional catalyst for the formation of AL or GVL from FF by using alcohols as the H-donors.

Reaction conditions: 0.2 g substrate, 20 mL solvent, 0.1 g Zr–Al/SBA-15(30:10), 453 K, 3 h and N_2 at atmospheric conditions. a: △Ho f (kJ/mol) is defined as the difference of the standard molar enthalpy of formation between the alcohol and the corresponding carbonyl compound, and the data from van der Waal et al. [46].

3.5. Leaching test and catalyst recycling study

Leaching and recycling tests were conducted to assess the stability and reusability of the catalyst. As expected, the yield of EL almost remained at a stable value after removing the catalyst at 1.5 h and continuing the reaction for another 1.5 h (Fig. 7a). This result disclosed that no significant leaching of active species from Zr–Al/SBA-15(30:10) catalyst during the reaction, which also confirmed by inductively coupled plasma-optical emission spectrometer (ICP-OES) (Table S3). The recycling test of Zr–Al/SBA-15(30:10) for the conversion of FF to EL was illustrated in Fig. 7b. Apparently, FF conversion and EL selectivity decreased to 75.5% and 62.2%, respectively in the first recycling test of the catalyst. Given the partial deactivation of the catalyst was probably attributed to carbon deposits during the reaction (Table S4), the used catalyst after the first cycle was regenerated by calcination at 823 K for 5 h. As can be seen in Fig. 7b, the second recycling test gave a comparable FF conversion to that in the case of fresh catalyst. A slight higher EL selectivity was also obtained than that in the first cycle, but still lower than that over the fresh catalyst. Furthermore, relatively stable FF conversion and EL selectivity were achieved in the third and fourth cycle.

The fresh, spent and regenerated catalysts were characterized by SEM and XRD to shine a light on the deactivation of the catalyst. Compared to the fresh catalyst, the similar morphology and specific surface area were observed in the spent and regenerated catalysts (Fig. S3 and Table S4), indicating that fundamental frame of SBA-15 kept intact after the reaction. However, the XRD profiles displayed that the diffraction lines for metal oxides became intensive for the spent and regenerated catalysts as compared to the fresh one (Fig. S6). This observation implied that agglomeration and/or sintering of active metal oxides should responsible for the partial deactivation of the spent and regenerated catalysts.

4. Conclusions

In this study, bi-functional Zr–Al/SBA-15 catalysts with varied ratios of ZrO_2 to Al_2O_3 were prepared for the cascade conversion of FF into EL through successive transfer hydrogenation and ethanolysis using ethanol as the in-situ hydrogen donor. Among these catalysts tested, Zr–Al/SBA-15(30:10) offered the optimal EL yield of 67.2% at 92.8% FF conversion under 453 K in 3 h, which is so far the highest EL yield from FF over non-noble metal catalysts. The superior catalytic performance of Zr–Al/SBA-15(30:10) should be attributed to the appropriate ratio (2.25) of Lewis and Brønsted acid sites over this catalyst, which allows efficient transfer hydrogenation and ethanolysis at the same time. Therefore, a facile one-pot process was developed for the conversion of FF to EL in this study based on a bifunctional Al/SBA-15(30:10) catalyst.

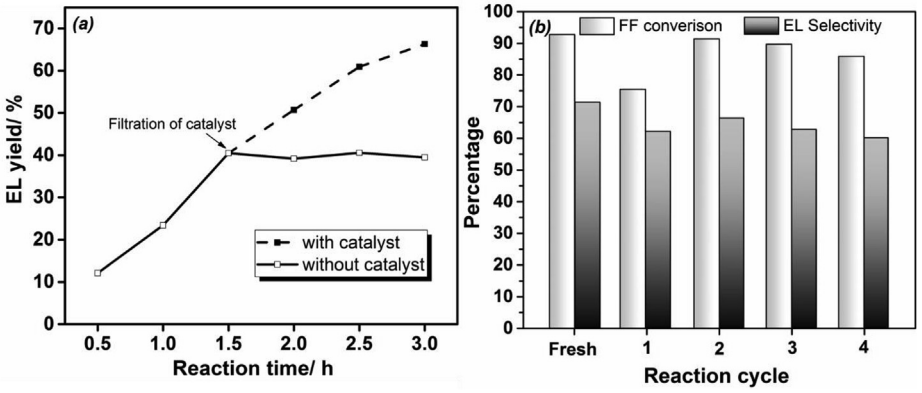

Fig. 7. Leaching test (a) and cycle reaction (b) of Zr–Al/SBA-15(30:10) in the conversion of FF to EL. Reaction conditions: 0.2 g FF, 20 mL ethanol, 0.1 g Zr–Al/SBA-15(30:10), 453 K, 3 h and N_2 at atmospheric conditions.

Acknowledgements

This work was supported by the National Natural Science Foundation of China (Grant Nos. 21676223; 21706223; 21776234), the Natural Science Foundation of Fujian Province of China (Grant No. 2018J01017), the Education Department of Fujian Province (Grant No. JZ160398) and the Energy Development Foundation of Energy College, Xiamen University (Grant No. 2017NYFZ02).

Appendix A. Supplementary data

Supplementary data to this article can be found online at https://doi.org/10.1016/j.renene.2019.09.064.

References

[1] L. Hu, A. Riisager, S. Saravanamurugan, A. Pandey, R. Sangwan, Y. Song, et al., Carbon-increasing catalytic strategies for upgrading biomass into energy-intensive fuels and chemicals, ACS Catal. 8 (1) (2017) 148–187.
[2] J.Y. Zhu, X. Pan, R.S. Zalesny, Pretreatment of woody biomass for biofuel production: energy efficiency, technologies, and recalcitrance, Appl. Microbiol. Biotechnol. 87 (3) (2010) 847–857.
[3] Y.C. Feng, M.Z. Li, Z.B. Gao, X. Zhang, X.H. Zeng, Y. Sun, et al., Development of betaine-based sustainable catalysts for green conversion of carbohydrates and biomass into 5-hydroxymethylfurfual, ChemSusChem 12 (2) (2019) 495–502.
[4] S.A. Arni, Comparison of slow and fast pyrolysis for converting biomass into fuel, Renew. Energy 124 (2018) 197–201.
[5] J. Liu, X.Q. Wang, B.B. Yang, C.L. Liu, C.L. Xu, W.S. Dong, Highly efficient conversion of glucose into methyl levulinate catalyzed by tin-exchanged montmorillonite, Renew. Energy 120 (2017) 231–240.
[6] E. Ahmad, M.I. Alam, K.K. Pant, M.A. Haider, Catalytic and mechanistic insights into the production of ethyl levulinate from biorenewable feedstocks, Green Chem. 18 (18) (2016) 4804–4823.
[7] C. Chang, L. Deng, G. Xu, Efficient conversion of wheat straw into methyl levulinate catalyzed by cheap metal sulfate in a biorefinery concept, Ind. Crops Prod. 117 (2018) 197–204.
[8] H. Joshi, B.R. Moser, J. Toler, W.F. Smith, T. Walker, Ethyl levulinate: a potential bio-based diluent for biodiesel which improves cold flow properties, Biomass Bioenergy 35 (7) (2011) 3262–3266.
[9] H.V. Srikanth, J. Venkatesh, S. Godiganur, S. Venkateswaran, B. Manne, Bio-based diluents improve cold flow properties of dairy washed milk-scum biodiesel, Renew. Energy 111 (2017) 168–174.
[10] T.Z. Lei, Z.W. Wang, X. Chang, L. Lin, X.Y. Yan, Y.C. Sun, et al., Performance and emission characteristics of a diesel engine running on optimized ethyl levulinate-biodiesel-diesel blends, Energy 95 (2016) 29–40.
[11] B.C. Windom, T.M. Lovestead, M. Mascal, E.B. Nikitin, T.J. Bruno, Advanced distillation curve analysis on ethyl levulinate as a diesel fuel oxygenate and a hybrid biodiesel fuel, Energy Fuel. 25 (4) (2011) 1878–1890.
[12] Z. Li, M. Zuo, Y. Jiang, X. Tang, X. Zeng, Y. Sun, et al., Stable and efficient CuCr catalyst for the solvent-free hydrogenation of biomass derived ethyl levulinate to γ-valerolactone as potential biofuel candidate, Fuel 175 (2016) 232–239.
[13] D. Ren, X. Wan, F. Jin, Z. Song, Y. Liu, Z. Huo, Selective hydrogenation of levulinate esters to 1,4-pentanediol using a ternary skeletal CuAlZn, Green Chem. 18 (22) (2016) 5999–6003.
[14] J.D. Vidal, M.J. Climent, A. Corma, D.P. Concepcion, S. Iborra, One-pot selective catalytic synthesis of pyrrolidone derivatives from ethyl levulinate and nitro compounds, ChemSusChem 10 (2017), 129-128.
[15] C. Song, S. Liu, X. Peng, J. Long, W. Lou, X. Li, Catalytic conversion of carbohydrates to levulinate ester over heteropolyanion-based ionic liquids, ChemSusChem 9 (23) (2016) 650–658.
[16] L. Peng, L. Lin, H. Li, Q. Yang, Conversion of carbohydrates biomass into levulinate esters using heterogeneous catalysts, Appl. Energy 88 (12) (2011) 4590–4596.
[17] X. Hu, C.-Z. Li, Levulinic esters from the acid-catalysed reactions of sugars and alcohols as part of a bio-refinery, Green Chem. 13 (7) (2011) 1676–1679.
[18] G. Xu, C. Chang, S. Fang, X. Ma, Cellulose reactivity in ethanol at elevate temperature and the kinetics of one-pot preparation of ethyl levulinate from cellulose, Renew. Energy 78 (2015) 583–589.
[19] K. Tominaga, A. Mori, Y. Fukushima, S. Shimada, K. Sato, Mixed-acid systems for the catalytic synthesis of methyl levulinate from cellulose, Green Chem. 13 (4) (2011) 810–812.
[20] G. Morales, A. Osatiashtiani, B. Hernández, J. Iglesias, J.A. Melero, M. Paniagua, et al., Conformal sulfated zirconia monolayer catalysts for the one-pot synthesis of ethyl levulinate from glucose, Chem. Commun. 50 (79) (2014) 11742–11745.
[21] H. Li, Z. Fang, R.L.S. Jr, S. Yang, Efficient valorization of biomass to biofuels with bifunctional solid catalytic materials, Prog. Energy Combust. Sci. 55 (2016) 98–194.
[22] Z. Zhang, K. Dong, Z.K. Zhao, Efficient conversion of furfuryl alcohol into alkyl levulinates catalyzed by an organic-inorganic hybrid solid acid catalyst, ChemSusChem 4 (1) (2011) 112–118.
[23] M.M. Antunes, P. Neves, A. Fernandes, S. Lima, A.F. Silva, M.F. Ribeiro, et al., Bulk and composite catalysts combining BEA topology and mesoporosity for the valorisation of furfural, Catal. Sci. Technol. 6 (21) (2016) 7812–7829.
[24] B. Chen, F. Li, Z. Huang, T. Lu, Y. Yuan, G. Yuan, Integrated catalytic process to directly convert furfural to levulinate ester with high selectivity, ChemSusChem 7 (1) (2014) 202–209.
[25] X. Tang, H. Chen, H. Lei, W. Hao, Y. Sun, X. Zeng, et al., Conversion of biomass to γ-valerolactone by catalytic transfer hydrogenation of ethyl levulinate over metal hydroxides, Appl. Catal., B 147 (1) (2014) 827–834.
[26] G.M. González Maldonado, R.S. Assary, J. Dumesic, L.A. Curtiss, Acid-catalyzed conversion of furfuryl alcohol to ethyl levulinate in liquid ethanol, Energy Environ. Sci. 5 (10) (2012) 8990–8997.
[27] X. Tang, Z. Li, X. Zeng, Y. Jiang, S. Liu, T. Lei, et al., In situ catalytic hydrogenation of biomass-derived methyl levulinate to γ-valerolactone in methanol, ChemSusChem 8 (9) (2015) 1601–1607.
[28] S. Zhu, Y. Cen, J. Guo, J. Chai, J. Wang, W. Fan, One-pot conversion of furfural to alkyl levulinate over bifunctional Au-$H_4SiW_{12}O_{40}/ZrO_2$ without external H_2, Green Chem. 18 (20) (2016) 5667–5675.
[29] L. Peng, X. Gao, X. Yu, H. Li, J. Zhang, L. He, Facile and high-yield synthesis of alkyl levulinate directly from furfural by combining Zr-MCM-41 and Amberlyst-15 without external H_2, Energy Fuel. 33 (1) (2018) 330–339.
[30] T. Kan, S. Xie, G.R. Cofield, X. Yang, E. Tian, H. Lin, Catalytic transfer hydrogenation of furfural for the production of ethyl levulinate: interplay of Lewis and Brønsted acidities, Energy Technol. 6 (2018) 1826–1831.
[31] M. Kruk, M. Jaroniec, Characterization of the porous structure of SBA-15, BioMed Res. Int. 12 (7) (2000) 945–953.
[32] L. Bui, H. Luo, W.R. Gunther, Y. Roman-Leshkov, Domino reaction catalyzed by zeolites with Brønsted and Lewis acid sites for the production of gamma-valerolactone from furfural, Angew. Chem. Int. Ed. 52 (31) (2013) 8022–8025.
[33] J. Du, H. Xu, J. Shen, J. Huang, W. Shen, D. Zhao, Catalytic dehydrogenation and cracking of industrial dipentene over M/SBA-15 (M = Al, Zn) catalysts, Appl. Catal., A 296 (2) (2005) 186–193.
[34] R. Huang, H. Yan, L. Li, D. Deng, Y. Shu, Q. Zhang, Catalytic activity of Fe/SBA-15 for ozonation of dimethyl phthalate in aqueous solution, Appl. Catal., B 106 (1) (2011) 264–271.
[35] S. Garg, K. Soni, G.M. Kumaran, M. Kumar, J.K. Gupta, L.D. Sharma, et al., Effect of Zr-SBA-15 support on catalytic functionalities of Mo, CoMo, NiMo hydrotreating catalysts, Catal. Today 130 (2) (2008) 302–308.
[36] X. Shi, Y. Wu, P. Li, H. Yi, M. Yang, G. Wang, Catalytic conversion of xylose to furfural over the solid acid SO_4^{2-}/ZrO_2-Al_2O_3/SBA-15 catalysts, Carbohydr. Res. 346 (4) (2011) 480–487.
[37] J. Zhao, Y. Yue, W. Hua, H. He, Z. Gao, Catalytic activities and properties of sulfated zirconia supported on mesostructured γ-Al_2O_3, Appl. Catal., A 336 (1) (2008) 133–139.
[38] Y.C. Feng, G.H. Yan, T. Wang, W.L. Jia, X.H. Zeng, J. Sperry, et al., Synthesis of MCM-41-supported metal catalysts in deep eutectic solvent for the conversion of carbohydrates into 5-hydroxymethylfurfural, ChemSusChem 12 (5) (2019) 978–982.
[39] Y. Wei, Y. Li, Y. Tan, J. Zhou, Z. Wu, Y. Liu, A facile route for one-pot synthesis of short-channeled bimetallic Zr–Al–SBA-15, Mater. Lett. 141 (2015) 145–148.
[40] A. Ramanathan, M.C. Castro Villalobos, C. Kwakernaak, S. Telalovic, U. Hanefeld, Zr-TUD-1: a Lewis acidic, three-dimensional, mesoporous, zirconium-containing catalyst, Chem. Eur J. 14 (3) (2010) 961–972.
[41] J. Sauer, F. Marlow, F. Schüth, Simulation of powder diffraction patterns of modified ordered mesoporous materials, Phys. Chem. Chem. Phys. 3 (24) (2001) 5579–5584.
[42] M. Espinosa, E. Terres, S. Pacheco, R. Mejia, R. Rodriguez, Sol–gel synthesis and characterization of SBA-15 in presence of metalloporphyrins: M-5, 10, 15, 20 TPP-Ni^{2+}, Etio-III-Ni^{2+} and Etio-III-Vo^{2+}, J. Sol. Gel Sci. Technol. 53 (2) (2010) 239–245.
[43] Dongyuan Zhao, Jinyu Sun, Quanzhi Li, D. Galen, Stucky. Morphological control of highly ordered mesoporous silica SBA-15, Chem. Mater. 12 (2) (2000) 275–279.
[44] J. Iglesias, J.A. Melero, G. Morales, M. Paniagua, B. Hernandez, A. Osatiashtiani, et al., ZrO_2-SBA-15 catalysts for the one-pot cascade synthesis of GVL from furfural, Catal. Sci. Technol. 8 (2018) 4485–4493.
[45] D. Das, H.K. Mishra, A.K. Dalai, K.M. Parida, Iron, and manganese doped SO_4^{2-}/ZrO_2 –TiO_2 mixed oxide catalysts: studies on acidity and benzene isopropylation activity, Catal. Lett. 93 (3–4) (2004) 185–193.
[46] J.C.V.D. Waal, P.J. Kunkeler, K. Tan, H.V. Bekkum, Zeolite titanium beta: a selective catalyst in the meerwein-ponndorf-verley-oppenauer reactions, Stud. Surf. Sci. Catal. 110 (1997) 1015–1024.